Inorganic Chemistry

Article

pubs.acs.org/IC

Positive Surface Charge Enhances Selective Cellular Uptake and Anticancer Efficacy of Selenium Nanoparticles

Bo Yu, Yibo Zhang, Wenjie Zheng,* Cundong Fan, and Tianfeng Chen*

Department of Chemistry, Jinan University, Guangzhou 510632, China

Supporting Information

ABSTRACT: Surface charge plays a key role in cellular uptake and biological actions of nanomaterials. Selenium nanoparticles (SeNPs) are novel Se species with potent anticancer activity and low toxicity. This study constructed positively charged SeNPs by chitosan surface decoration to achieve selective cellular uptake and enhanced anticancer efficacy. The results of structure characterization revealed that hydroxyl groups in chitosan reacted with SeO_3^{2-} ion to form special chain-shaped intermediates, which could be decomposed to form crystals upon reduction by ascorbic acid. The initial colloids nucleated and then assembled into spherical SeNPs. The positive charge of the NH_3^+ group on the outer surface of the nanoparticles contributed to the high stability in aqueous solutions. Moreover, a panel of four human cancer cell lines were found to be susceptible to SeNPs, with IC_{50} values ranging from 22.7 to 49.3 μM. Chitosan surface decoration of SeNPs significantly enhanced the selective uptake by endocytosis in cancer cells and thus amplified the anticancer efficacy. Treatment of the A375 melanoma cells with chitosan−SeNPs led to dose-dependent apoptosis, as evidenced by DNA fragmentation and phosphatidylserine translocation. Our results suggest that the use of positively charged chitosan as a surface decorator could be a simple and attractive approach to achieve selective uptake and anticancer action of nanomaterials in cancer cells.

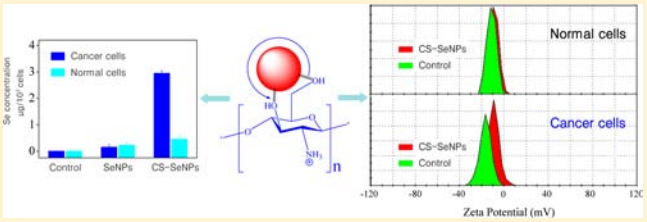

INTRODUCTION

Chemotherapy refers to the use of cytotoxic agents or materials to inhibit, reverse, or retard tumorigenesis, by targeting fast growing cells and blocking some critical elements in the process of cell growth or by promoting cancer cell apoptosis.[1] It is a cost-effective approach to reduce cancer morbidity and mortality through inhibition of precancerous events before the clinical occurrence of the disease.[2] However, many studies have demonstrated that pharmacologically active drugs reached the tumor tissue with poor specificity, thus resulting in unavoidable side effects. Nanotechnology is a growing field of science that utilizes the physicochemical properties of nanomaterials as a means to achieve unique applications in mesoscopic physics and medicine.[3] The basic rationale is that nanoscaled materials have optical, magnetic, or structural properties that are not available from molecules or bulk solids.[4,5] The combination of biotechnology and nanotechnology has led to the development of an interdisciplinary area, bionanotechnology, which has broad applications in molecular imaging, molecular diagnosis, and targeted therapy.[6] The development of cancer bionanotechnology opens novel horizons for diagnosis and therapy of diseases that have traditionally been recognized as incurable via basic therapies or surgical methods, such as malignant cancers.[7] Recently, nanoscaled delivery vehicles, such as nanoparticles and nanorods, have been used in drug delivery systems to enhance their therapeutic efficacy, due to their ability to promote local delivery and controlled drug release.[8] By confinement the cytotoxic action of the anticancer drugs within the malignant tissues, nanoscaled delivery systems are foreseen as potential chemotherapeutic techniques that could lead to focused destruction of the cancerous cells.[9]

Selenium (Se) is a trace element with wide commercial applications, due to its novel chemical and physical properties, such as piezoelectricity, photoconductivity, thermoelectricity, and nonlinear optical responses.[10] The role of Se in cancer chemoprevention and chemotherapy has been supported by many epidemiological, preclinical, and clinical studies.[11] Much effort has been devoted to fabrication of Se nanomaterials, including nanoparticles, nanorods, nanowires, and nanotubes, using physical vapor deposition, vapor phase diffusion, and wet chemical methods.[12−14] Se nanoparticles (SeNPs) attracted more and more attention in the past decade due to their high bioavailability and antioxidant activities, low toxicity, and novel therapeutic properties.[15−19] Compared with organic and inorganic selenocompounds, elemental Se exhibited potential for local delivery of high doses into cancer cells due to its higher density.[20] Functionalized SeNPs could be internalized by cancer cells through endocytosis, which induced apoptotic cell death by triggering mitochondria-mediated apoptosis pathways.[17−19,21] Nowadays, SeNPs have been regarded as a potent Se species for cancer chemoprevention and chemotherapy. Nevertheless, the low selectivity between cancer and normal

Received: May 20, 2012
Published: August 9, 2012

   dx.doi.org/10.1021/ic301050v | *Inorg. Chem.* 2012, 51, 8956−8963

cells greatly hinders the further development of SeNPs as anticancer agents.

Biomacromolecules have been widely used in precise synthesis of inorganic nanomaterials through control of the process of crystal nucleation and the growth of nanomaterials.[22] Polysaccharides are macromolecules with a high diversity of molecular structures that could be used as soft templates for synthesis of nanomaterials. For instance, polysaccharides have been applied in preparation of nanoparticles to prevent plasma protein adsorption, maximize circulation time, and enhance cell-penetrating ability.[8] Chitosan (CS), a cationic polysaccharide composed of randomly distributed (1,4)-linked 2-amino-2-deoxy-β-D-glucose units, has been utilized to fabricate Au, Ag, ZnS, and CdS nanomaterials.[23−26] Owing to its special properties, including nontoxicity, high biodegradability and biocompatibility, and novel antimicrobial activity, CS has been applied in biosensing, medicine, and pharmaceutics.[27,28] The NH_3^+ groups in CS on the surface could interact with the phosphoryl groups of phospholipid components in cell membrane, thus enhancing the binding of the nanoparticles to the cell membrane and increasing their internalization.[29] Nevertheless, little information about the use of CS as a capping agent for SeNPs is available.

Many studies have found that the physicochemical properties of nanomaterials have significant biological implications in their cellular uptake and biological processes.[30] The size and surface charge could affect the cellular uptake efficiency and pathways of inorganic and polymeric materials by influencing the adhesion and interaction of the nanoparticles with the cell membrane.[31−33] Intracellular uptake of nanoparticles is a complicated process, with the involvement of adhesion to cells followed by an internalization process. Surface decoration of nanoparticles by biomacromolecules could facilitate the cellular uptake by enhancing the adhesion of nanoparticles to the cell membrane due to their biological adhesion properties.[18,27] Interestingly, studies have found that nanoparticles with higher positive charge exhibited stronger affinity for the negatively charged cell membrane, thus accounting for higher cellular uptake.[34] It is not hard to infer that distinct cell surface properties and nanoparticle surface charges could result in cell-line-specific uptake and selective biological action. Therefore, in the present study, we aimed to synthesize size-controlled and stable SeNPs capped with CS with a positive charge to achieve selective cellular uptake and enhanced anticancer efficacy. Our results revealed that the chemical structure and the physicochemical properties of CS played key roles in the formation and action of the SeNPs. Moreover, the positive surface charge from the NH_3^+ group in CS significantly enhanced the cell membrane-permeating abilities and apoptosis-inducing activities of SeNPs.

EXPERIMENTAL SECTION

Reagents and Materials. Selenium dioxide, 3-(4,5-dimethylthiazol-2-yl)-2,5-diphenyltetrazolium bromide (MTT), propidium iodide (PI), solid JC-1,2′,7′-dichlorofluorescein diacetate (DCF-DA), and ascorbic acid were purchased from Sigma-Aldrich Chemical Co. The Annexin-V-FLUOS staining kit and in situ cell death detection kits were obtained from Roche Molecular Biochemicals. The water used for all experiments was ultrapure, supplied by a Milli-Q water purification system from Millipore. All of the solvents used were of HPLC grade. Chitosan, with a molecular weight of 60 000 g/mol and degree of deacetylation of 90.0%, was purchased from Beijing Ribio Biotech Co., Ltd.

Preparation and Characterization of CS-SeNPs. The solution of CS was prepared by dissolving 1 g of CS powder with 1 g of acetic acid in 100.0 mL of Milli-Q water. The solution of 100 mM ascorbic acid was freshly prepared. As a typical procedure, varied volume of CS solution was added dropwise into 1 mL of 125 M H_2SeO_3 solution under magnetic stirring, and then 5 mL of 100 mM ascorbic acid solution was added into the mixture, and it was reconstituted to a final volume of 25 mL with Milli-Q water. The final concentration of Se was 5 mM, and the reactant concentrations of CS were 0.01, 0.08, 0.16, 0.32, and 0.48 mg/mL. The solution was dialyzed against Milli-Q water until no Se was detected in the outer solution by ICP-AES analysis.

The shapes and crystalline structures of as-prepared products were characterized using microscopic and spectroscopic methods. Briefly, TEM samples were prepared by dispersing the powder particles onto holey carbon films on copper grids. The micrographs were obtained on Hitachi H-7650 for TEM operated at an accelerating voltage at 80 kV. And the Philips TECNAI 20 high-resolution transmission electron microscopy (HRTEM) worked at 400 kV. SEM-EDX analysis was carried out on an EX-250 system (Horiba) and employed to examine the elemental composition of CS-SeNPs. The size distribution of the nanoparticles was measured by PCS on a Nano-ZS instrument (Malvern Instruments Limited). Fourier transform infrared spectroscopy (FT-IR) spectra of the samples were recorded on Equinox 55 IR spectrometer in the range 4000−400 cm^{-1} using the KBr-disk method.

To determine the *in vitro* cellular uptake of CS-SeNPs, the nanoparticles containing a fluorescent dye, 6-coumarin, were prepared using a similar procedure, except that 6-coumarin (4 μg/mL) was added to the reaction system after the addition of CS. After reacting for 24 h under room temperature, the solution was dialyzed against Milli-Q water 3 times. The incorporated dye acts as a probe for CS-SeNPs and offers a sensitive method to determine their intracellular uptake and localization.

Measurement of ζ Potential. The ζ potential of suspended cells was analyzed with a Nano-ZS instrument. Cells were seeded in tissue culture plates at a density of 5×10^4 cells/mL for 12 h. The cells were then incubated with CS-SeNPs at 20 μM concentrations for 2 h. Cells were collected by 0.25% trypsin detachment and washed with PBS 2 times. All cell samples were resuspended in PBS, and the ζ potential of suspended cells or spheroids was measured on a Nano-ZS instrument 3 times.

Determination of Se. Se concentration was determined by the ICP-AES method. Briefly, the sample was digested with 3 mL of concentrated nitric acid and 1 mL of H_2O_2 in a digestive stove (Qian Jian Measuring Instrument Co., Ltd., China) at 180 °C for 3 h. The digested product was reconstituted to 10 mL with Milli-Q H_2O and used for ICP-AES analysis.

Cell Lines and Cell Culture. Several human cancer cell lines, including A375 melanoma cells, HepG2 hepatocellular carcinoma cells, MG63 osteosarcoma cells, and HK-2 human immortalized proximal tubule epithelial cells, were purchased from American Type Culture Collection (ATCC, Manassas, VA). All cell lines were maintained in either RPMI-1640 or DMEM media supplemented with fetal bovine serum (10%), penicillin (100 units/mL), and streptomycin (50 units/mL) at 37 °C in CO_2 incubator (95% relative humidity, 5% CO_2).

MTT Assay. Cell viability was determined by measuring the ability of cells to transform MTT to a purple formazan dye.[35] Cells were seeded in 96-well tissue culture plates at 2.5×10^3 cells/well for 24 h. The cells were then incubated with CS-SeNPs at different concentrations for different periods of time. After incubation, 20 μL/well of MTT solution (5 mg/mL in PBS) was added and incubated for 5 h. The medium was aspirated and replaced with 150 μL/well of DMSO. The color intensity of the formazan solution, which reflects the cell growth condition, was measured at 570 nm using a microplate spectrophotometer (Versamax).

Flow Cytometric Analysis. The cell cycle distribution was analyzed by flow cytometry as previously described.[36] After treatment with CS-SeNPs, the cells were trypsinized, washed with PBS, and fixed with 70% ethanol overnight at −20 °C. The fixed cells were washed with PBS and stained with PI working solution (1.21 mg/mL Tris, 700

dx.doi.org/10.1021/ic301050v | Inorg. Chem. 2012, 51, 8956−8963

U/mL RNase, 50.1 μg/mL PI, pH 8.0) for 4 h in darkness. The stained cells were analyzed with Epics XL-MCL flow cytometer (Beckman Coulter, Miami, FL). Cell cycle distribution was analyzed using MultiCycle software (Phoenix Flow Systems, San Diego, CA). The proportion of cells in G0/G1, S, and G2/M phases was represented as DNA histograms. Apoptotic cells with hypodiploid DNA content were measured by quantifying the sub-G1 peak in the cell cycle pattern. For each experiment, 10 000 events per sample were recorded.

TUNEL-DAPI Co-staining Assay. DNA fragmentation induced by CS-SeNPs was examined by using an *in situ* cell death detection kit following the manufacturer's protocol.[37] Briefly, the cells cultured in chamber slides were fixed with 3.7% formaldehyde and then permeabilized with 0.1% Triton X-100 in PBS. The cells were incubated with TUNEL reaction mixture for 1 h. For nuclear staining, cells were incubated with 1 μg/mL of DAPI for 15 min at 37 °C. Stained cells were then washed with PBS and examined on a fluorescence microscope (Nikon Eclipse 80i).

Annexin-V-FLUOS Staining Assay. Detection of plasma membrane alterations in cells treated with CS-SeNPs was performed using annexin-V-FLUOS staining assay as described previously.[38] The cells were seeded in an eight-chamber polystyrene vessel (Becton Dickinson Labware) and incubated for 24 h. After addition of CS-SeNPs to the culture medium, incubation continued for an additional 24 h. Cells were then stained with annexin-V-FLUOS labeling solution (annexin-V−fluorescein in Hepes buffer containing PI) for 15 min. The slides were directly analyzed by confocal microscopy (Bio-Rad Radiance 2100MP scanning system equipped with 488 nm argon laser), and fluorescence images were captured using LaserShape 2000 software. Excitation and emission wavelengths were set at 488 and 515 nm, respectively.

Determination of Intracellular Se Concentration. Intracellular Se concentration was determined by the ICP-AES method as previously described.[38] Briefly, collected cells were digested with 3 mL of concentrated nitric acid and 1 mL of H_2O_2 in an infrared rapid digestion system (Gerhardt) at 180 °C for 1.5 h. The digested solution was reconstituted to 10 mL with Milli-Q H_2O and used for ICP-AES analysis.

Intracellular Localization of CS-SeNPs. The intracellular localization of CS-SeNPs in A375 cells was traced with the lysosomal marker Lyso Tracker Red staining. Briefly, the cells cultured on a cover glass in 6-well plates until 70% confluence were stained with 80 nM lyso-tracker DND-99 (Molecular Probes) and 1 μg/mL DAPI for 2 h and 20 min, respectively. After washing with PBS twice, the cells were incubated with different concentrations of 6-coumarin-labeled CS-SeNPs for various periods of time and examined under a fluorescence microscope (Nikon Eclipse 230 80i).

Statistical Analysis. All experiments were carried out at least in triplicate, and results were expressed as mean ± SD. Statistical analysis was performed using SPSS statistical program version 13 (SPSS Inc., Chicago, IL). The difference between the two groups was analyzed by two-tailed Student's *t*-test. Difference with $P < 0.05$ (*) was considered statistically significant. The difference between three or more groups was analyzed by one-way ANOVA multiple comparisons.

RESULTS AND DISCUSSION

Preparation and Characterization of CS-SeNPs. Nanoparticles with size ranging from 30 to 150 nm were more favorably produced to enhance the cellular uptake.[39] Thus, it was meaningful to control the size of nanomaterials. In the present study, size-controlled SeNPs were prepared by adding CS to the redox system of selenite acid and ascorbic acid. Figure 1A−C shows the TEM images of the as-prepared CS-SeNPs with the absence (A) and presence of 0.08 (B) and 0.48 mg/mL CS (C), which clearly revealed that SeNPs decorated with 0.08 mg/mL CS presented monodisperse and homogeneous spherical structure with an average diameter of about 120 nm. In contrast, SeNPs without CS easily aggregated and

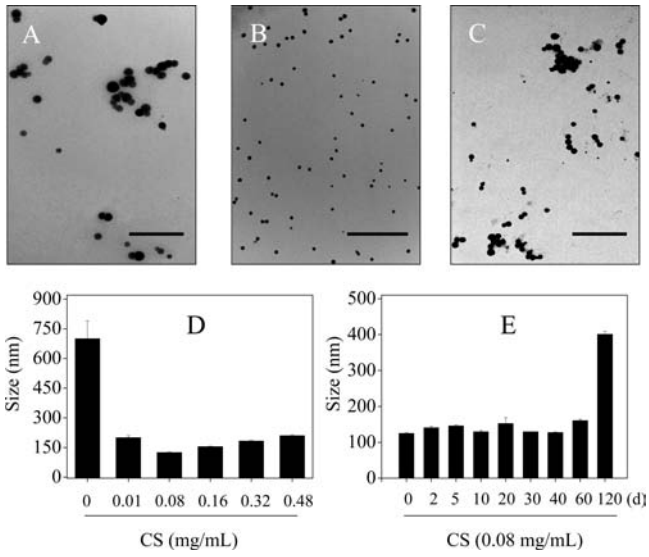

Figure 1. TEM images of SeNPs in the absence (A) and presence of CS at 0.08 (B) and 0.48 mg/mL (C). (D, E) Size distribution of CS-SeNPs. Scar bar 1 μm.

precipitated in the aqueous solutions (Figure 1A) and thus showed an average diameter of 700 nm (Figure 1D). In contrast, the presence of CS at 0.01−0.48 mg/mL significantly decreased the particle diameters to 200, 120, 154, 183, and 209 nm, respectively. It was also found that the CS-SeNPs remained stable at least for 60 days when stored in 0.08 mg/mL CS solutions (Figure 1E). However, when the reaction time increased to 120 days, the size of CS-SeNPs dramatically increased to 401 nm, and aggregation of the critical nuclei began to happen. Sedimentation plays an important role in the cellular uptake of nanomaterials;[40] therefore, the stability of CS-SeNPs supports their medicinal applications.

The products were further characterized by SEM-EDX and high-resolution transmission electron microscopy (HRTEM). The results of SEM (Figure 2A) showed that the particle morphology of CS-SeNPs has been achieved with large quantities and the particle size distributed between 100 and 150 nm with an average diameter of 120 nm. Moreover, HRTEM was used to examine the distance between parallel lattice planes of the as-obtained nanoparticles. Figure 2B shows the lattice pattern of the SeNPs obtained at room temperature, which revealed that the value was 0.149 nm. In addition, an amorphous coating layer of several nanometers width (marked with a white box in Figure 2B) was observed on the surface of a mineralized NP cores, indicating that the CS was probably incorporated into SeNPs, which was consistent with the result of FT-IR. An elemental composition analysis employing SEM-EDX showed the presence of strong signals from the Se atoms (85.5%), together with C atom signal (12.1%) and O atom signal (2.4%) from CS (Figure 2C). As shown in Figure 2D, the FT-IR spectrum of CS-SeNPs resembled that of CS, giving evidence that CS has formed a part of the nanocomposite. In the spectrum of CS, the peaks at 3430 cm^{-1} was attributed to the O−H stretching vibration, while the peaks at 2928, 2958, and 1647 cm^{-1} corresponded to the stretching vibrations of C−H, C−C, and C−N groups, respectively. The appearance of the above peaks in the spectrum of CS-SeNPs confirmed the presence of CS on the surface of SeNPs. Moreover, the characteristic peak of −OH group in CS-SeNPs nanocomposites at 3426.2 cm^{-1} was relatively lower than that of

dx.doi.org/10.1021/ic301050v | Inorg. Chem. 2012, 51, 8956−8963

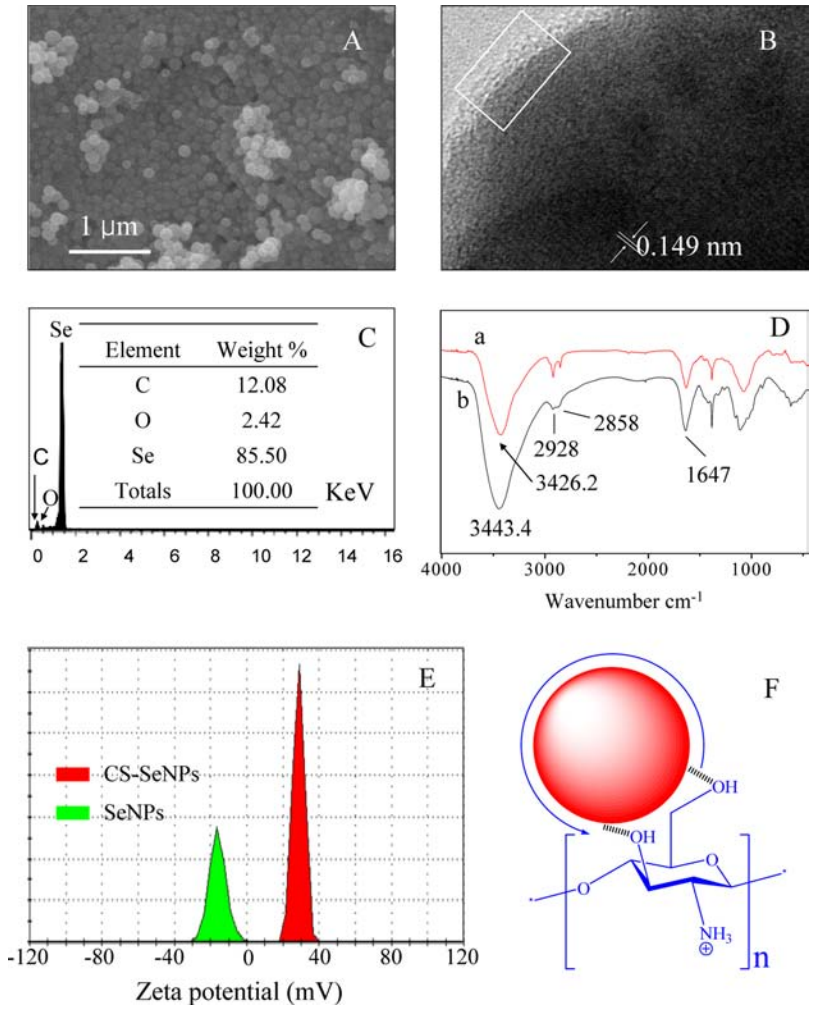

Figure 2. Characterization of CS-SeNPs: (A) SEM, (B) HRTEM, and (C) SEM-EDX analysis of CS-SeNPs; (D) FT-IR spectra of CS-SeNPs (a) and CS (b); (E) ζ potential distribution of CS-SeNPs and SeNPs; (F) proposed structure of CS-SeNPs.

CS (3443.4 cm^{-1}), with blue-shift observed, indicating that CS was conjugated to the surface of SeNPs through the −OH group. The significance of ζ potential can be related to the stability of colloidal dispersion, which also indicates the degree of repulsion between adjacent and similarly charged particles. A high ζ potential will confer high stability of colloidal dispersion. In this study, we found that the value of the ζ potential of the CS-SeNPs was +29.1 mV and that of SeNPs was −16.2 mV (Figure 2E), which suggest that the highly positive-charged NH_3^+ groups were exposed on the outside surface of SeNPs.

On the basis of these results, we proposed that the chemical structure and the physicochemical properties of CS play key roles in the growth of the Se nanostructures. The −OH group in the CS molecule reacts with SeO_3^{2-} anions to form special chain-shaped intermediates, which could be decomposed to form Se crystals upon reduction with ascorbic acid. Furthermore, the initial colloid system could be nucleated with CS surface decoration and then assembled onto spherical SeNPs. As shown in Figure 2F, CS was conjugated to SeNPs through −OH groups, and the positive charge of the NH_3^+ group on the outer surface of the nanoparticles contributed to the high stability of CS-SeNPs in aqueous solutions. The appropriate amount of CS in the solutions helps to control the growth of SeNPs and thus prevent Ostwald ripening and precipitation.

In Vitro Cellular Uptake and Localization of CS-SeNPs.

An important factor that usually contributes to nanomaterial-based drug cytotoxicity is cellular uptake.[41] Many studies have shown that slight physicochemical differences between nanomaterials has significant biological implications in cellular uptake and biological processes. For instance, particle size and surface charge can affect the efficiency of cellular uptake for liposomes, quantum dots, polymeric NPs, gold NPs, and silica NPs by influencing the adhesion of the particles and their interaction with cells.[42] In this study, we propose a technique to overcome the passive transport drawbacks of nanomaterials by introducing a biological soft molecule, CS, with a positive charge to the surface of SeNPs to enhance their selective uptake and anticancer action. Before starting the experiments, we have examined the size distribution of CS-SeNPs in PBS. As shown in Figure S1, Supporting Information, CS-SeNPs remained stable in PBS solution for at least 10 days, with the size ranging from 120 to 150 nm, which supports the stability of CS-SeNPs in *in vitro* cell studies. Since A375 cells exhibited the highest sensitivity to CS-SeNPs (Figure 3 A), this cell line was used for investigation of the cellular uptake and intracellular fate of the nanomaterials. First, the interaction between CS-SeNPs and human cells was characterized by changes in ζ potential. Figure 3B shows that human cells were negatively charged. The surface ζ potential for HK-2 human normal cells and A375 melanoma

dx.doi.org/10.1021/ic301050v | *Inorg. Chem.* 2012, 51, 8956−8963

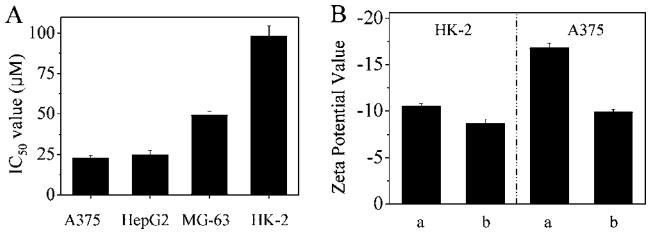

Figure 3. *In vitro* anticancer activities of CS-SeNPs and the ζ potential of suspended cells: (A) Growth inhibition of CS-SeNPs on selected human cancer and normal cell lines (72 h). Cell viability was determined by a colorimetric MTT assay. Each IC_{50} value represents the mean ± SD of three independent experiments. (B) The ζ potential of suspended HK-2 and A375 cells in the absence (a) and presence (b) of 20 μM CS-SeNPs.

cells were −10.5 ± 0.3 and −16.8 ± 0.5 mV, respectively. Uptake of CS-SeNPs led to the change of ζ potential to −8.7 ± 0.4 and −9.9 ± 0.3 mV for HK-2 and A375 cells, respectively. These results demonstrate different interaction intensity between CS-SeNPs with positive charge and distinct human cells. It is possible that the higher negative charge in A375 cells would lead to stronger interaction with CS-SeNPs and result in higher cellular uptake and stronger cytotoxic effects.

To confirm this hypothesis, we examined the cellular uptake of CS-SeNPs in A375 cells and HK-2 cells treated for 24 h by using ICP-AES analysis. As shown in Figure 4, A375 cells

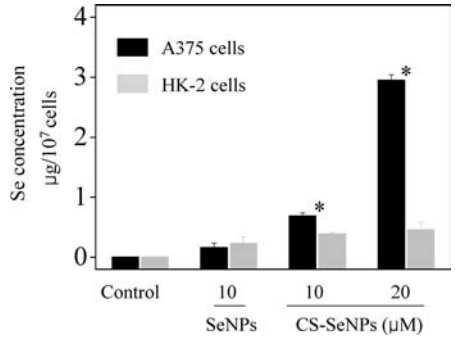

Figure 4. Quantitative analysis of Se concentrations in A375 cells and HK-2 cells exposed to SeNPs and CS-SeNPs for 24 h by ICP-AES method. Significant difference between A375 and HK-2 cells is indicated at $P < 0.05$ (*) level.

treated with 10 and 20 μM CS-SeNPs had significantly increased Se concentrations, from 0.0046 (control) to 0.69 and 2.95 $\mu g/10^7$ cells, which was significantly higher than that of SeNPs without CS decoration (0.16 $\mu g/10^7$ cells). Interestingly, in HK-2 cells, it was found that treatments with 10 and 20 μM CS-SeNPs only increased the Se concentrations from 0.0040 (control) to 0.39 and 0.46 $\mu g/10^7$ cells, which was significantly lower than those in A375 cancer cells. Taken together, our results suggest that the smaller size and the positive surface charge contributed to the enhanced cellular uptake of CS-SeNPs, compared with SeNPs, in cancer cells.

Endocytosis was one of the most important entry mechanisms that influenced the biodistribution for extracellular materials, particularly nanomaterials. In this study, the localization CS-SeNPs in A375 cancer cells was investigated by using specific probes, Lyso Tracker Red and DAPI, for fluorescence imaging of lysosomes and cell nucleus, respectively. As shown in Figure 5, the combination of blue, red, and

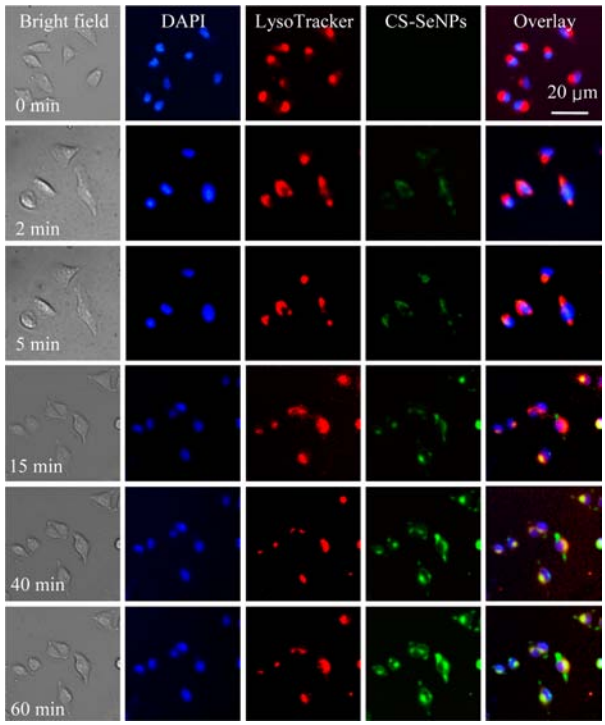

Figure 5. Intracellular fate of CS-SeNPs. A375 cells labeled with DAPI (nucleus) and Lyso Tracker Red (lysosome) were treated with 6-coumarin-loaded nanoparticles at 37 °C for different periods of time and visualized under fluorescence microscope.

green fluorescence clearly indicates the colocalization of CS-SeNPs and lysosomes in A375 cells after 5 min, which increased in a time-dependent manner. CS-SeNPs escaped from lysosomes after 15 min and then were released into cytosol and distributed in cells after 40 min. During the whole process, the fluorescence from CS-SeNPs could not be observed in the nucleus. These results suggest that lysosomes are the main target organelles of CS-SeNPs.

***In Vitro* Anticancer Activity of CS-SeNPs.** The *in vitro* cytotoxic effects of CS-SeNPs were screened against various human cancer cell lines by means of MTT assay. As shown in Figure 3A, cellular uptake of CS-SeNPs resulted in broad spectrum growth inhibition against A375, HepG2, and MG-63 cells with IC_{50} values ranging from 22.7 to 49.3 μM. Despite this potency, CS-SeNPs showed lower cytotoxicity toward normal human kidney cells (HK-2) with an IC_{50} value of 98.29 μM, which was much higher than that in A375, HepG2, and MG-63 cancer cells. These results suggest that CS-SeNPs possess great selectivity between cancer and normal cells and display potential application in cancer chemoprevention and chemotherapy. This selectivity should be due to different electric interaction intensity between CS-SeNPs and distinct human cells. It is possible that the higher negative charge in A375 cells would lead to stronger interaction with CS-SeNPs with positive charge and result in higher cellular uptake and stronger cytotoxic effects.

Based on the chemical composition of CS-SeNPs as examined by EDX analysis, we compared the cytotoxicity of SeNPs, CS, and CS-SeNPs against the most susceptible A375 cells at corresponding concentrations to examine the enhancement of CS on the anticancer action of SeNPs. As shown in Figure 6A, treatments of CS-SeNPs inhibited the growth of A375 cells in a time- and dose-dependent manner. For instance,

dx.doi.org/10.1021/ic301050v | *Inorg. Chem.* 2012, 51, 8956−8963

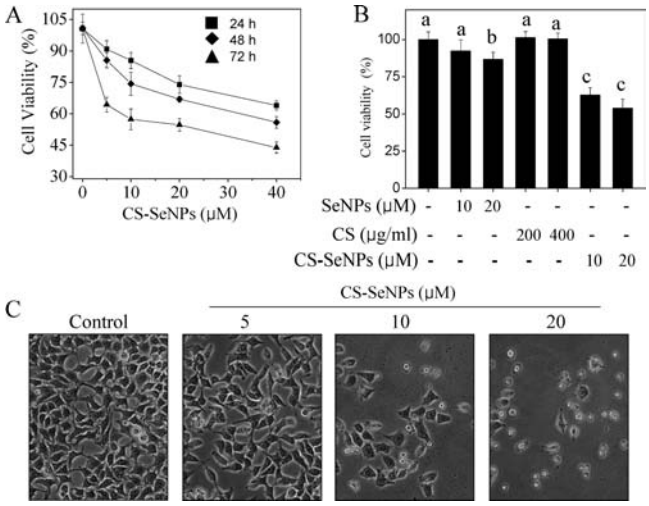

Figure 6. (A) Cell viability after treatment with different concentrations of CS-SeNPs for 24, 48, and 72 h as examined by MTT assay. (B) Growth inhibition of SeNPs, CS, and CS-SeNPs against the most susceptible A375 cells. Cell viability was determined by a colorimetric MTT assay. Cells were treated with various concentrations of samples for 72 h. (C) Morphology of A375 cells treated with CS-SeNPs for 72 h (magnification, 200×).

CS-SeNPs at concentrations of 10 and 20 μM significantly decreased the cell viability to 62.7% and 53.8% of control group, respectively. Under the corresponding conditions, SeNPs at the same concentrations only slightly decreased the cell viability to 92.3% and 86.7%, whereas CS at 200 and 400 μg/mL showed no cytotoxicity toward A375 cells (Figure 6B). Moreover, under the same concentrations, the mixture of CS and SeNPs showed much lower cytotoxicity toward A375 cells compared with CS-SeNPs (Figure S2, Supporting Information). These results clearly demonstrate that CS surface decoration significantly enhanced the anticancer activity of SeNPs. Moreover, the results of phase-contrast observation (Figure 6C) show that A375 cells treated with CS-SeNPs for 72 h exhibited dose-dependent reduction in cell numbers, loss of cell-to-cell contact, cell shrinkage and formation of apoptotic bodies, which suggest the induction of apoptotic cell death by CS-SeNPs.

Induction of Apoptosis by CS-SeNPs in Cancer Cells. The inhibition of cancer cell proliferation by anticancer drugs could be the result of induction of apoptosis or cell cycle arrest or a combination of these two modes. Therefore, we performed PI-flow cytometric analysis to determine what mechanisms were involved in the cell death induced by CS-SeNPs. The results reveal that exposure of A375 cells to different concentrations of CS-SeNPs led to dose-dependent increase in the proportion of apoptotic cells, as reflected by the sub-G1 populations (Figure 7). For instance, treatment of A375 cells with 20 μM CS-SeNPs increased the sub-G1 peak from 2.6% (control) to 79.1%. In contrast, no significant changes in cell cycle distribution of G0/G1, S, and G2/M phases were observed in treated cells. Apoptotic cell death was further confirmed by DNA fragmentation and nuclear condensation as examined by TUNEL and DAPI co-staining assay. DNA fragmentation has been regarded as an important biochemical hallmark of cell apoptosis. TUNEL staining is an effective way to detect early stage DNA fragmentation in apoptotic cells prior to changes in morphology.

As shown Figure 8, the green and blue color corresponded to TUNEL and DAPI staining, respectively. After exposure of the cells to CS-SeNPs for 24 h, A375 cells exhibited dose-dependent increase in DNA fragmentation, nuclear condensation and formation of apoptotic bodies. Translocation of phosphatidylserine to the outer leaflet of the plasma membrane plays a critical role in phagocytosis of apoptotic cells, which has been recognized as an important characteristic of cell apoptosis. Thus, in the present study, Annexin-V staining assay was performed to confirm induction of cell apoptosis by CS-SeNPs. As shown in Figure 9, CS-SeNPs caused dose-dependent increase in proportions of apoptotic cells (annexin-V positive).

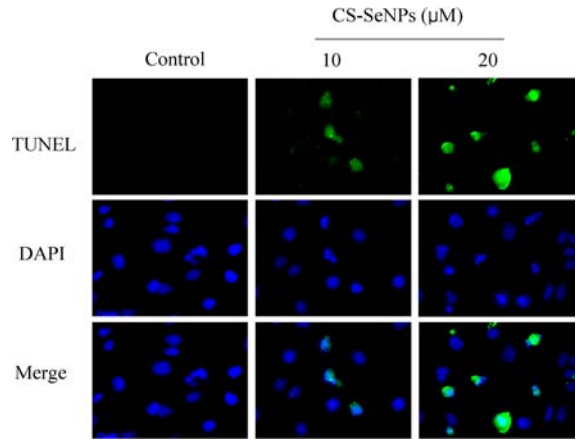

Figure 8. DNA fragmentation and nuclear condensation induced by CS-SeNPs in A375 cells revealed by TUNEL–DAPI co-staining assay. Cells were treated with CS-SeNPs for 24 h. Magnification, 200×.

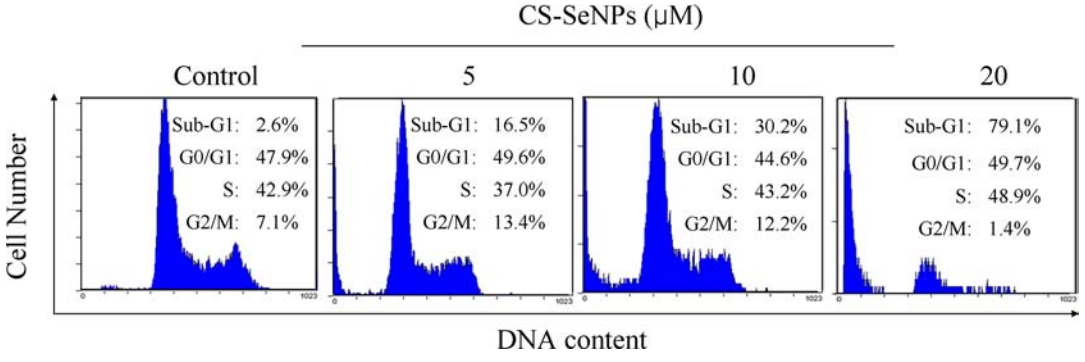

Figure 7. Flow cytometric analysis of apoptosis and change in cell cycle distribution of A375 cells treated with CS-SeNPs for 72 h.

dx.doi.org/10.1021/ic301050v | Inorg. Chem. 2012, 51, 8956–8963

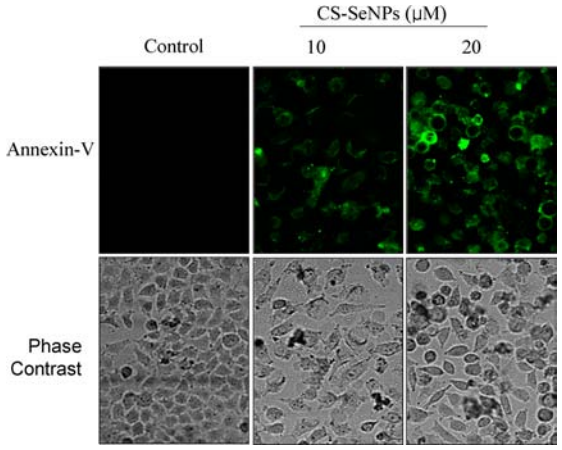

Figure 9. Examination of phosphatidylserine translocation by annexin-V-FLUOS staining assay. Cells were exposed to CS-SeNPs for 24 h. Magnification, 200×.

Taken together, these results demonstrate that the major mode of cell death induced by CS-SeNPs is cell apoptosis.

CONCLUSION

A simple method for synthesis of size-controlled and stable SeNPs capped by positively charged CS to achieve enhanced cellular uptake and anticancer efficacy has been demonstrated in this study. Spherical CS-SeNPs with striking stability were prepared under the optimized conditions. CS surface decoration significantly enhanced the cellular uptake and cytotoxicity of Se-NPs in human cancer cells. The studies on the underlying molecular mechanisms revealed that the major mode of cell death induced by CS-SeNPs was cell apoptosis. Our results suggest that the use of positively charged chitosan as surface decorator could be a simple and attractive approach to achieve selective uptake and anticancer action of nanomaterials in cancer cells.

ASSOCIATED CONTENT

Supporting Information

Experimental details for the size distribution of CS-SeNPs in PBS and *in vitro* cellular studies of mixture of CS and SeNPs. This material is available free of charge via the Internet at http://pubs.acs.org.

AUTHOR INFORMATION

Corresponding Author

*Fax: +86-20-85221263. E-mail: tzhwj@jnu.edu.cn (W.J.Z); tchentf@jnu.edu.cn (T.F.C).

Notes

The authors declare no competing financial interest.

ACKNOWLEDGMENTS

This work was supported by National Science and Technology support program, Natural Science Foundation of China and Guangdong Province, the Fundamental Research Funds for the Central Universities, Program for New Century Excellent Talents in University, and the Doctoral Foundation of Ministry of Education of China.

REFERENCES

(1) Pan, M.-H.; Ho, C.-T. *Chem. Soc. Rev.* **2008**, *37*, 2558–2574.
(2) Chen, C.; Kong, A. N. T. *Trends Pharmacol. Sci.* **2005**, *26*, 318–326.
(3) Yu, B.; Chen, T.; Yang, F.; Liu, W.; Li, Y.-H.; Zheng, W. *Chem. Lett.* **2011**, *40*, 242–243.
(4) Nel, A.; Xia, T.; Madler, L.; Li, N. *Science* **2006**, *311*, 622–627.
(5) Craig, G. E.; Brown, S. D.; Lamprou, D. A.; Graham, D.; Wheate, N. J. *Inorg. Chem.* **2012**, *51*, 3490–3497.
(6) Nie, S. M.; Xing, Y.; Kim, G. J.; Simons, J. W. *Annu. Rev. Biomed. Eng.* **2007**, *9*, 257–288.
(7) Rozhkova, E. A.; Ulasov, I.; Lai, B.; Dimitrijevic, N. M.; Lesniak, M. S.; Rajh, T. *Nano Lett.* **2009**, *9*, 3337–3342.
(8) Ferrari, M. *Nat. Rev. Cancer* **2005**, *5*, 161–171.
(9) Acharya, S.; Dilnawaz, F.; Sahoo, S. K. *Biomaterials* **2009**, *30*, 5737–5750.
(10) Zhang, C. M.; Yang, J.; Quan, Z. W.; Yang, P. P.; Li, C. X.; Hou, Z. Y.; Lin, J. *Cryst. Growth Des.* **2009**, *9*, 2725–2733.
(11) Sinha, R.; Ei-Bayoumy, K. *Curr. Cancer Drug Targets* **2004**, *4*, 13–28.
(12) Bai, Y.; Wang, Y. D.; Zhou, Y. H.; Li, W. J.; Zheng, W. J. *Mater. Lett.* **2008**, *62*, 2311–2314.
(13) Kaur, G.; Iqbal, M.; Bakshi, M. S. *J. Phys. Chem. C* **2009**, *113*, 13670–13676.
(14) Xie, Q.; Dai, Z.; Huang, W. W.; Zhang, W.; Ma, D. K.; Hu, X. K.; Qian, Y. T. *Cryst. Growth Des.* **2006**, *6*, 1514–1517.
(15) Tan, L.; Jia, X. e.; Jiang, X.; Zhang, Y.; Tang, H.; Yao, S.; Xie, Q. *Biosens. Bioelectron.* **2009**, *24*, 2268–2272.
(16) Li, Y. H.; Li, X. L.; Wong, Y. S.; Chen, T. F.; Zhang, H. B.; Liu, C. R.; Zheng, W. J. *Biomaterials* **2011**, *32*, 9068–9076.
(17) Yang, F.; Tang, Q. M.; Zhong, X. Y.; Bai, Y.; Chen, T. F.; Zhang, Y. B.; Li, Y. H.; Zheng, W. J. *Int. J. Nanomed.* **2012**, *7*, 835–844.
(18) Wu, H. L.; Li, X. L.; Liu, W.; Chen, T. F.; Li, Y. H.; Zheng, W. J.; Man, C. W. Y.; Wong, M. K.; Wong, K. H. *J. Mater. Chem.* **2012**, *22*, 9602–9610.
(19) Zhang, Y.; Li, X.; Huang, Z.; Zheng, W.; Fan, C.; Chen, T. *Nanomed. Nanotechnol. Biol. Med.* **2012**, DOI: 10.1016/j.nano.2012.04.002.
(20) Sarin, L.; Sanchez, V. C.; Yan, A.; Kane, A. B.; Hurt, R. H. *Adv. Mater.* **2010**, *22*, 5207–5211.
(21) Chen, T.; Wong, Y.-S.; Zheng, W.; Bai, Y.; Huang, L. *Colloids Surf. B* **2008**, *67*, 26–31.
(22) Lee, S.; Kwon, C.; Park, B.; Jung, S. *Carbohydr. Res.* **2009**, *344*, 1230–1234.
(23) Zhu, A. P.; Yuan, L. H.; Jin, W. J.; Dai, S.; Wang, Q. Q.; Xue, Z. F.; Qin, A. J. *Acta Biomater.* **2009**, *5*, 1489–1498.
(24) Esumi, K.; Takei, N.; Yoshimura, T. *Colloids Surf. B* **2003**, *32*, 117–123.
(25) Miyama, T.; Yonezawa, Y. *Langmuir* **2004**, *20*, 5918–5923.
(26) Wu, L.; Shi, C.; Tian, L.; Zhu, J. *J. Phys. Chem. C* **2007**, *112*, 319–323.
(27) Zhang, X. K.; Meng, L. J.; Lu, Q. G.; Fei, Z. F.; Dyson, P. J. *Biomaterials* **2009**, *30*, 6041–6047.
(28) Jayakumar, R.; Menon, D.; Manzoor, K.; Nair, S. V.; Tamura, H. *Carbohydr. Polym.* **2010**, *82*, 227–232.
(29) Liu, H.; Du, Y. M.; Wang, X. H.; Sun, L. P. *Int. J. Food Microbiol.* **2004**, *95*, 147–155.
(30) Matsuno, R.; Ishihara, K. *Nano Today* **2011**, *6*, 61–74.
(31) Lin, J. Q.; Zhang, H. W.; Chen, Z.; Zheng, Y. G. *ACS Nano* **2010**, *4*, 5421–5429.
(32) Luo, J.; Chan, W. B.; Wang, L. Y.; Zhong, C. J. *Int. J. Antimicrob. Agents* **2010**, *36*, 549–556.
(33) Xu, F.; Yuan, Y.; Shan, X. Q.; Liu, C. S.; Tao, X. Y.; Sheng, Y.; Zhou, H. J. *Int. J. Pharm.* **2009**, *377*, 199–206.
(34) He, C. B.; Hu, Y. P.; Yin, L. C.; Tang, C.; Yin, C. H. *Biomaterials* **2010**, *31*, 3657–3666.
(35) Chen, T. F.; Wong, Y. S. *J. Agric. Food Chem.* **2008**, *56*, 10574–10581.
(36) Chen, T. F.; Wong, Y. S. *Int. J. Biochem. Cell Biol.* **2009**, *41*, 666–676.

(37) Chen, T.; Liu, Y.; Zheng, W.-J.; Liu, J.; Wong, Y.-S. *Inorg. Chem.* **2010**, *49*, 6366−6368.
(38) Chen, T. F.; Wong, Y. S. *Biomed. Pharmacother.* **2009**, *63*, 105−113.
(39) Thorek, D. L. J.; Tsourkas, A. *Biomaterials* **2008**, *29*, 3583−3590.
(40) Cho, E. C.; Zhang, Q.; Xia, Y. N. *Nat. Nanotechnol.* **2011**, *6*, 385−391.
(41) Li, C.; Yang, K.; Zhang, Y.; Tang, H.; Yan, F.; Tan, L.; Xie, Q.; Yao, S. *Acta Biomater.* **2011**, *7*, 3070−3077.
(42) He, C.; Hu, Y.; Yin, L.; Tang, C.; Yin, C. *Biomaterials* **2010**, *31*, 3657−3666.